Sensitivity of the ocean's deep overturning circulation to easterly Antarctic winds

Andrew L. Stewart[1] and Andrew F. Thompson[1]

Received 13 July 2012; revised 10 August 2012; accepted 11 August 2012; published 21 September 2012.

[1] We investigate the sensitivity of the deep meridional overturning circulation (MOC) in the Southern Ocean to changes in the easterly wind stress over the Antarctic continental slope. The deep MOC is driven by export of dense Antarctic Bottom Water from the Antarctic continental shelf, and exerts a strong influence on climate by ventilating the deep ocean with oxygen and storing carbon dioxide. The possibility that inter-climatic modifications of the deep overturning may have been driven by changes in the atmospheric circulation has motivated the recent interest in evaluating the sensitivity of the Southern Ocean MOC to modifications of the mid-latitude westerlies. Using a high-resolution eddy-resolving model of a sector of the Southern Ocean, we show that the deep cell of the MOC is highly sensitive to the strength of the polar easterlies, and relatively insensitive to the strength of the mid-latitude westerlies. Our results highlight that determining the deep ocean ventilation in past and future climates demands an accurate evaluation of the concurrent surface wind stress throughout the Southern Ocean. **Citation:** Stewart, A. L., and A. F. Thompson (2012), Sensitivity of the ocean's deep overturning circulation to easterly Antarctic winds, *Geophys. Res. Lett.*, *39*, L18604, doi:10.1029/2012GL053099.

1. Introduction

[2] The ocean's meridional overturning circulation (MOC) is responsible for the global transport of dynamical tracers such as heat and salt, and biogeochemical tracers such as oxygen and carbon [*Lumpkin and Speer*, 2007]. It is central to our understanding of both the modern climate [*Kuhlbrodt et al.*, 2007], and that of the last glacial maximum [*Lynch-Stieglitz et al.*, 2007]. *Marshall and Speer* [2012] have recently highlighted the essential role of wind-driven upwelling in the Southern Ocean in closing the upper cell of the MOC by providing a path for deep water masses to return to the surface. This article addresses a second, closely-related contribution of the Southern Ocean to the MOC: the export of Antarctic Bottom Water (AABW).

[3] Water that upwells to the surface of the Southern Ocean is either transported north by surface currents and subducted as Antarctic Intermediate Water (AAIW), or transported south towards the Antarctic continental shelf [*Speer et al.*, 2000]. In certain regions, largely confined to the Weddell and Ross Seas, the upwelled water mixes with fresh glacial meltwater, and high-salinity shelf water produced by rejection of brine during sea ice formation [*Gordon*, 2009]. The resulting mixture sinks down from the continental shelf and spreads throughout the global ocean as Antarctic Bottom Water (AABW). This downwelling carries oxygen to the deep ocean; anoxic events in past climates have been attributed to stagnation of this circulation [*Hotinski et al.*, 2001]. The ventilation of CO_2 from the deep MOC may also account for the rise in atmospheric pCO_2 since the last glacial maximum (LGM) [*Skinner et al.*, 2010].

[4] A poleward shift in the mid-latitude westerlies has been proposed as the initiator of the CO_2 ventilation from the deep ocean since the LGM [*Toggweiler*, 2009]. Meanwhile, the intensification and poleward shift of the southern hemisphere westerlies over the last 50 years has been attributed to anthropogenic CO_2 emissions [*Shindell and Schmidt*, 2004; *Polvani et al.*, 2011]. This has motivated a series of investigations into the sensitivity of the Antarctic Circumpolar Current (ACC) and its overturning circulation to changes in the strength and position of the mid-latitude westerlies [*Meredith et al.*, 2011; *Abernathey et al.*, 2011]. The westerly wind stress curl drives a mean overturning circulation via Ekman pumping at the base of the surface mixed layer, and tends to shoal isopycnals to the south [*Döös and Webb*, 1994]. This overturning is counteracted by eddies generated via baroclinic instability, which act to transport tracers along density surfaces, and thereby relax the isopycnal slopes [*Abernathey et al.*, 2011]. The observed stratification and MOC may be regarded as the residual of the competing mean and "eddy" overturning circulations [*Marshall and Radko*, 2003]. Modelling studies disagree on whether the additional input of westerly momentum intensifies the MOC, or whether stronger eddy fluxes compensate for the stronger Ekman pumping [*Hofmann and Morales Maqueda*, 2011]. Observations suggest that the stratification of the Southern Ocean has not changed over the past decades in response to the intensification of the westerlies [*Böning et al.*, 2008].

[5] The objective of this article is to highlight that the MOC, in particular the deep lower overturning cell, may be strongly sensitive to changes in the polar easterly winds. These blow directly along the Antarctic continental shelf [*Large and Yeager*, 2009] and drive the Antarctic Slope Front (ASF) current at the shelf break [*Jacobs*, 1991]. As such, we may expect the export of bottom water and the deep overturning circulation to be more sensitive to modification of the polar easterlies than of the mid-latitude westerlies. The strengthening of the Southern Annular Mode over the past decades [*Thompson et al.*, 2000] has intensified the polar vortex, but the trend in the polar easterlies over the Antarctic continental slope is ambiguous [*Polvani et al.*, 2011]. Modelling studies of the LGM climate suggest that the strength of

[1]Environmental Sciences and Engineering, California Institute of Technology, Pasadena, California, USA.

Corresponding author: A. L. Stewart, Environmental Sciences and Engineering, California Institute of Technology, Pasadena, CA 91125, USA. (stewart@gps.caltech.edu)

0094-8276/12/2012GL053099

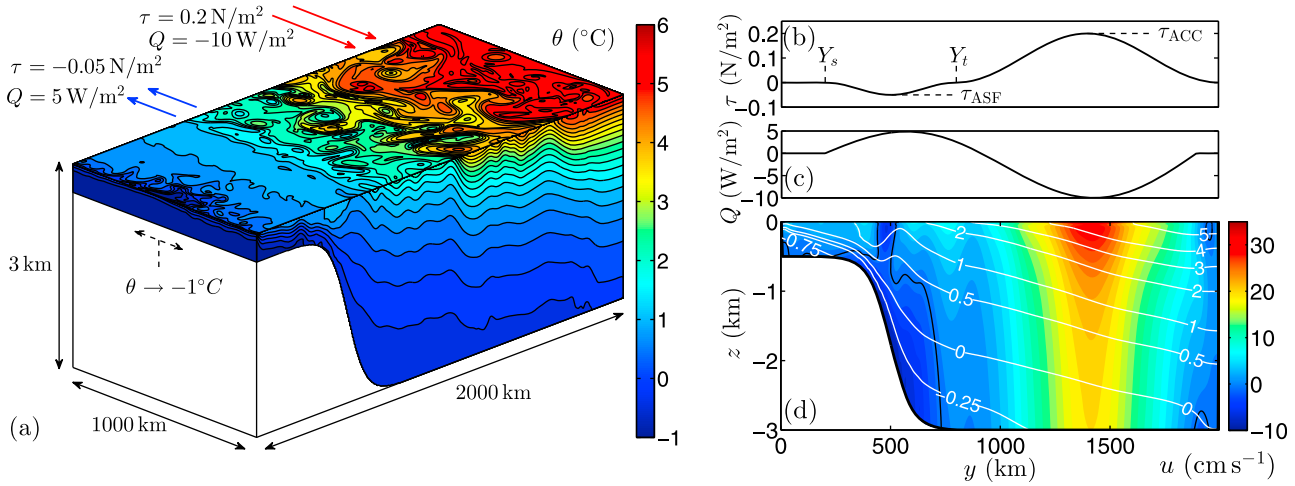

Figure 1. Simulation set-up. The model ocean depth ranges from 500 m at the southern boundary to 3000 m in the north, via a continental slope of width ∼200 km at y = 500 km. (a) A snapshot of the instantaneous model temperature, with the magnitudes of imposed surface forcings indicated above. (b and c) The surface wind stress and heat flux profiles, where positive Q corresponds to heat flux from the ocean to the atmosphere. (d) The time- and zonal-mean temperature (contours) and zonal velocity (colours). The black contour separates regions of eastward (positive) and westward (negative) flow.

the polar easterlies differed substantially from present day, but with considerable variation around the Antarctic continental shelf [*Kitoh et al.*, 2001]. Here we examine the sensitivity of the MOC to variations in the strength of the polar easterlies using an idealized model that captures the main features of the circulation.

2. High-Resolution Simulations of the Antarctic Continental Shelf and Slope

[6] We conduct our simulations using the MIT ocean general circulation model (MITgcm) [*Marshall et al.*, 1997], which solves numerically the three-dimensional, hydrostatic, Boussinesq equations [*Vallis*, 2006]. We model the ACC, ASF and Antarctic continental shelf as a periodic, walled zonal channel, illustrated in Figure 1a. The dimensions of our channel have been chosen to agree qualitatively with the shape of the continental shelf in the western Weddell Sea, though for computational efficiency our model is somewhat shallower than the ∼4000 m -depth of the real Southern Ocean. For simplicity we neglect the roughness of the bathymetry and the variation of density with salinity, imposing a constant thermal expansion coefficient $\alpha = 2 \times 10^{-4}$ K^{-1}. A localized source of dense water is provided at the southern boundary via linear relaxation of the shelf temperature towards $\theta_c = -1$°C within a ∼200 km radius of $x = y = 0$. The shortest relaxation timescale is 1 week, and is imposed at $x = y = 0$, $z = -500$ m. This idealized parametrisation of bottom water formation neglects both salinity and the nonlinearity of the equation of state. However, our aim is not to simulate bottom water formation, but rather to analyze the export of dense water from the continental shelf and its contribution to the MOC.

[7] The model is forced at the surface using a steady, zonally-symmetric zonal wind stress, described by

$$\tau(y) = \begin{cases} \tau_{\mathrm{ACC}} \sin^2\left(\dfrac{\pi(y - Y_t)}{L_y - Y_t}\right), & Y_t \le y \le L_y, \\ \tau_{\mathrm{ASF}} \sin^2\left(\dfrac{\pi(Y_t - y)}{Y_t - Y_s}\right), & Y_s \le y \le Y_t, \end{cases} \quad (1)$$

and $\tau = 0$ over $0 \le y \le Y_s$. This profile allows independent variation of the easterly and westerly wind strengths, whilst ensuring continuity of both the wind stress and the wind stress curl at the shelf $y = Y_s$ and at the transition $y = Y_t$. Here τ_{ASF} and τ_{ACC} measure the strengths of the polar easterlies and mid-latitude westerlies respectively. In our reference simulation we used $\tau_{\mathrm{ACC}} = 0.2$ Nm^{-2}, $\tau_{\mathrm{ASF}} = -0.05$ Nm^{-2}, $Y_s = 200$ km, and $Y_t = 800$ km.

[8] We also impose a steady, zonally-symmetric surface temperature flux that acts to heat the surface of the ACC and cool the surface close to the continental shelf. The surface wind and temperature forcing profiles are plotted in Figures 1b and 1c, and approximate the observed surface forcing over the Southern Ocean [*Large and Yeager*, 2009]. The southernmost 200 km of the surface is not forced. We use the K-profile parametrisation (KPP) for vertical mixing [*Large et al.*, 1994] to provide a well-mixed surface layer of depth ∼50 m. The momentum imparted to the surface via wind stress is extracted via a linear bottom friction of strength $r_b = 1.1 \times 10^{-3}$ ms^{-1}. Over the northern 100 km of the domain we relax the temperature towards an exponential profile that ranges from 0°C at $z = -3000$ m to 6°C at $z = 0$ with a temperature scale height of 1000 m. The shortest relaxation timescale is 1 week at $y = 2000$ km. This profile has been chosen to match approximately the profile obtained in simulations without relaxation at the northern boundary, and represents the restoration of the stratification by diabatic processes that parameterize water mass transformations occuring at more northern latitudes [*Abernathey et al.*, 2011].

[9] In all of the results described below the flow is subject to a constant gravitational acceleration $g = 9.81$ ms^{-2}, and to a Coriolis force with reference rotation $f_0 = 1 \times 10^{-4}$ s^{-1} and meridional gradient $\beta = 1 \times 10^{-11}$ m^{-1} s^{-1}. The dynamical equations are discretized on a horizontal grid of 204 by 400 points, with a grid spacing of approximately 5 km. This grid spacing is much smaller than the first internal Rossby radius of deformation in the ACC (∼20 km) and comparable to that on the continental shelf (∼5 km), but simulations run

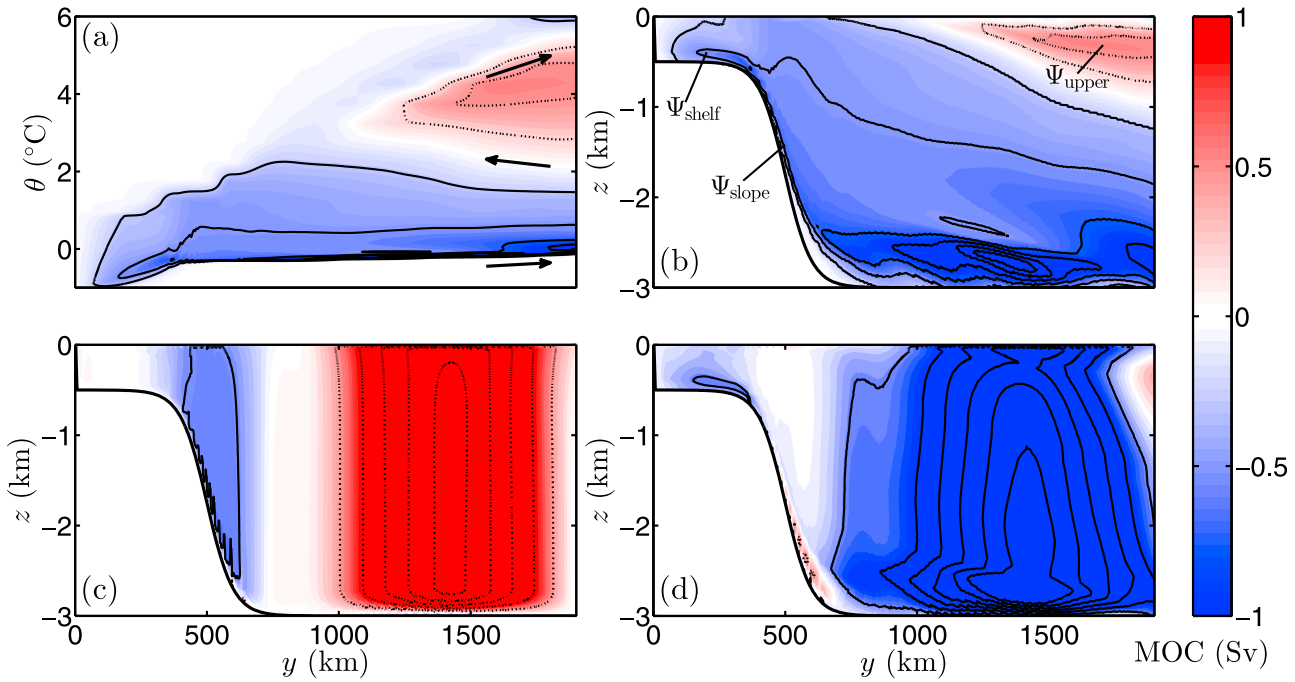

Figure 2. Plots of (a) the MOC (ψ) in y/θ coordinates, and (b) mapped back to y/z coordinates. (c and d) The mean (ψ_{mean}) and eddy (ψ_{eddy}) components of the MOC, where $\psi = \psi_{\text{mean}} + \psi_{\text{eddy}}$. The color scale measures the MOC strength in Sv. Positive (dashed) and negative (solid) streamlines are plotted with a contour interval of 0.25 Sv in Figures 2a and 2b, and a contour interval of 0.5 Sv in Figures 2c and 2d. In Figure 2a the arrows indicate the direction of the transport, whilst in Figure 2b we illustrate our MOC quantifiers, described in §4.

at resolutions as fine as 2 km yield almost identical results. The vertical grid consists of 30 points with spacings ranging from 12.5 m in the surface mixed layer to 187.5 m in the lowest grid cell, and partial cells are used to improve the vertical resolution of the continental slope. Mixing by subgridscale eddies is represented by a horizontal viscosity $A_h = 12\ \text{m}^2\ \text{s}^{-1}$, a vertical viscosity $A_v = 3 \times 10^{-4}\ \text{m}^2\ \text{s}^{-1}$, and a vertical mixing of temperature $\kappa_v = 5 \times 10^{-6}\ \text{m}^2\ \text{s}^{-1}$. Grid-scale biharmonic and Leith viscosities were also included for numerical stability [*Leith et al.*, 1996].

[10] Our reference simulation yields a system of zonal currents that are similar to the real ACC and ASF, shown in Figure 1d. The model ACC lies between $y \approx 800$ km and $y = 2000$ km, and is characterized by surface-intensified velocities due to thermal-wind balance with temperature contours that shoal to the south [*Vallis*, 2006]. The ~410 Sv ($1\ \text{Sv} = 1 \times 10^6\ \text{m}^3\ \text{s}^{-1}$) zonal transport of the model ACC is much larger than the estimated ~130 Sv transport of the real ACC [*Nowlin and Klinck*, 1986] because the momentum input at the surface is balanced only by friction at the flat bottom, rather than form drag due to bathymetry [*Ferreira et al.*, 2005]. However, the model's baroclinic transport of ~80 Sv is close to the baroclinic transport of the ACC, and the simulated temperature stratification is similar to that of the real ocean. The meridionally-shoaled isotherms in Figure 1d are baroclinically unstable, and this generates the turbulent field of eddies visible in Figure 1a [*Vallis*, 2006]. These eddies counteract steepening of the isotherms due to wind-driven Ekman pumping in the surface mixed layer [*Marshall and Radko*, 2003]. Our simulations reproduce the observed V-shaped dip in the isopycnals at the ASF, with slopes somewhat steeper than the observations of *Thompson and Heywood* [2008] and shallower than those of *Muench and Gordon* [1995] in the western Weddell Sea. The maximum westward velocity of ~8 cms^{-1} in the model ASF lies at the lower end of the range of velocities observed around the Antarctic continent [*Jacobs*, 1991], but is comparable to the measurements of *Muench and Gordon* [1995]. Increasing the strength of the easterlies to $\tau_{\text{ASF}} = -0.1\ \text{Nm}^{-2}$ yields a velocity maximum of ~25 cms^{-1}, comparable to the observations of *Thompson and Heywood* [2008].

3. Dense Water Outflow and Overturning

[11] We analyze the meridional circulation of our reference experiment using an overturning streamfunction defined by the time- and zonal-mean mass fluxes within isothermal layers [*Döös and Webb*, 1994; *Abernathey et al.*, 2011],

$$\psi(y,\theta) = \overline{\left\langle \int_{z=0}^{\theta'=\theta} v\, \mathrm{d}z \right\rangle}. \tag{2}$$

Here we employ shorthands for averages in time, $\langle \bullet \rangle \equiv T^{-1} \int_{t_0}^{t_0+T} \bullet\, \mathrm{d}t$, and zonal integrals, $\bar{\bullet} \equiv \oint \bullet\, \mathrm{d}x$. For all results described here the averaging period is $T = 30$ yr, and the total kinetic energy of the flow has reached a statistically steady state prior to the initial time t_0. Volume transports in the ocean interior tend to be aligned with the instantaneous isothermal surfaces [*Marshall and Radko*, 2003], so that ψ is an effective quantifier of the net meridional flux at a given temperature. We plot the streamfunction (2) calculated for

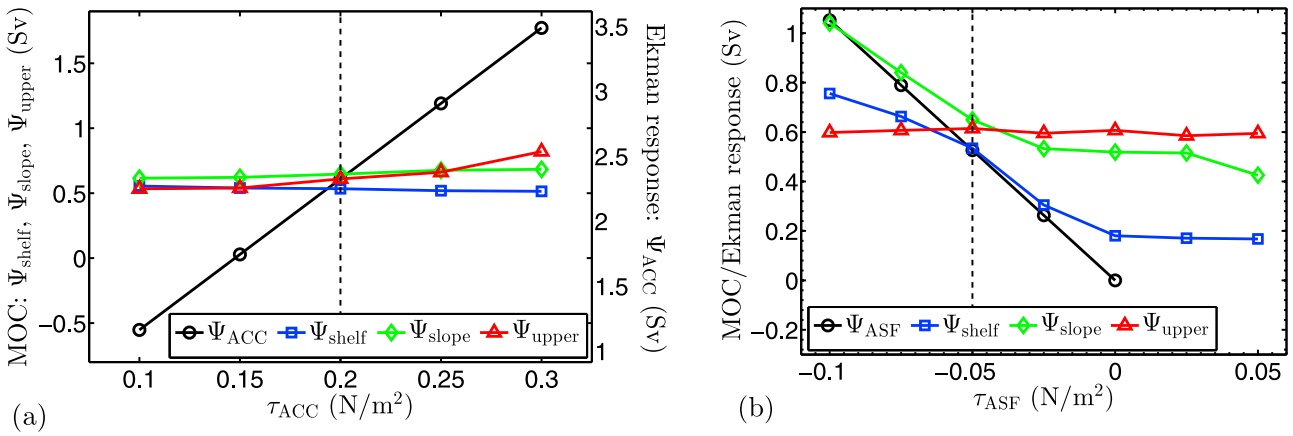

Figure 3. Sensitivity of dense water export from the continental shelf (Ψ_{shelf}) and slope (Ψ_{slope}), and of the strength of the upper overturning cell (Ψ_{upper}), to changes in the surface wind stress. (a) We vary the strength of the mid-latitude westerlies, and (b) the strength of the polar easterlies. Dashed lines indicate the reference simulation. For comparison, we also plot the theoretical wind-driven overturning strengths Ψ_{ACC} and Ψ_{ASF} in Figures 3a and 3b respectively. In Figure 3a we plot Ψ_{ACC} over an offset range of overturning strengths to allow visual comparison of the gradients of Ψ_{ACC}, Ψ_{shelf}, Ψ_{slope} and Ψ_{upper}.

our reference experiment in Figure 2a, whilst Figure 2b shows an approximate mapping of ψ back to y/z-coordinates [*McIntosh and McDougall*, 1996]. To analyze the contribution of eddies to the MOC, we also define the mean and "eddy" overturning streamfunctions following *Nurser and Lee* [2004] and *Abernathey et al.* [2011],

$$\psi_{mean}(y,\theta) = \overline{\int_{z=0}^{\theta'=\theta} \langle v \rangle dz}, \qquad \psi_{eddy} = \psi - \psi_{mean}. \tag{3}$$

The mean overturning measures the meridional transport along isopycnals by the time-mean velocity. In Figure 2c we plot ψ_{mean} mapped back to y/z coordinates. In the interior, ψ_{mean} is almost exactly the theoretical wind-driven circulation due to Ekman pumping in the surface mixed layer, which we denote as $\psi_{Ekman} = -\tau L_x/\rho_0 f$ [*Marshall and Radko*, 2003]. The discrepancy between ψ and ψ_{mean} is the result of the strong eddy streamfunction ψ_{eddy}, due to fluctuations of the velocity and temperature around their time-mean states. Eddy stirring is strongly constrained by density surfaces and tends to smooth out gradients in the thickness of isopycnal layers, resulting in a net mass transport [*Marshall and Speer*, 2012]. We plot ψ_{eddy} mapped to y/z coordinates in Figure 2d.

[12] Figure 2a illustrates the distinctive split of the MOC into upper and lower overturning cells. The MOC is aligned with the isotherms in the near-adiabatic ocean interior, but crosses them rapidly in the surface mixed layer due to strong diapycnal mixing. The upper overturning cell consists of mid-depth waters that upwell to the surface within outcropping isotherms, before being transported northwards and subducted again by the imposed surface heat flux. The lower overturning cell is sustained by waters that upwell further south, where the surface cooling drives them southward. This circulation draws dense water off the shelf and then down the continental slope, where an intense basal overturning cell transports it rapidly northwards across the ACC. Note this deep overturning is squeezed in temperature space in Figure 2a. The deep recirculation in the ACC is the result of the intense diapycnal mixing that occurs when outcropping isotherms are transported rapidly across the ocean bed by eddies. The tendency of bottom friction to retard the flow at the base causes the isotherms to steepen and overflow, leading to a statically unstable temperature profile that activates the convective parametrization (KPP). Decreasing the vertical sizes of the grid cells to 100 m reduces the strength of the deep recirculation by around 1/3, but the overturning in the upper ACC and over the continental shelf and slope varies by no more than 2%. If this channel were extended around a ~17, 000 km latitude band at 65°S then typical MOC strengths in both the upper and lower cells would be around 10 Sv, which is similar to the estimate of *Lumpkin and Speer* [2007].

[13] Figures 2c and 2d show that in the ACC, the MOC is accurately characterized as a small "residual" of strong mean and eddy circulations ψ_{mean} and ψ_{eddy} [*Marshall and Radko*, 2003; *Abernathey et al.*, 2011]. By contrast, on the continental shelf ($y \leq 200$ km) there is no wind-driven overturning because no surface wind stress is imposed, and the export of dense water is dominated by ψ_{eddy}. Over the continental slope the MOC is dominated by the wind-driven mean overturning ψ_{mean}. The weak eddy activity over the slope is consistent with the suppression of baroclinic instability over a sloping bottom [*Isachsen*, 2011]. When the wind stress over the ASF reverses (easterly to westerly), the strength of ψ_{eddy} over the slope becomes comparable to ψ_{mean} (not shown).

4. Sensitivity to Surface Wind Stress

[14] We now explore the sensitivity of the model's MOC to the strengths of the polar easterlies and mid-latitude westerlies. We quantify the strength of the upper MOC cell as the maximum value of ψ over the domain [*Abernathey et al.*, 2011], which we denote as Ψ_{upper}. To quantify the strength of the lower MOC, we consider all streamlines that stretch continuously from the equatorward edge of the AABW formation region (y = 200 km) to the poleward edge of the northern relaxation region (y = 1900 km). We define Ψ_{shelf} as the largest value of $|\psi|$ over all such streamlines. This measures the transport of water from the

continental shelf to the northern boundary, and the return transport from the northern boundary to the shelf, but excludes the influence of flows that recirculate close to the ocean bed. We define Ψ_{slope} identically, but over streamlines that stretch continuously between y = 500 km and y = 1900 km. This measures the transport between the continental slope and the northern boundary, and more accurately quantifies the strength of the lower MOC in cases where water mass exchange with the continental shelf is suppressed.

[15] In Figure 3 we plot the dependence of Ψ_{shelf}, Ψ_{slope} and Ψ_{upper} on the wind strength parameters τ_{ACC} and τ_{ASF}. For each variation of the wind stress profile shown in Figure 3, we hold all other simulation parameters fixed and integrate forward in time until the model's total kinetic energy reaches a statistically steady state. We compute ψ via (2) using a 30-year time average, and then calculate Ψ_{shelf}, Ψ_{slope} and Ψ_{upper} as described above. We also quantify the strengths of the theoretical wind-driven mean overturning using the maximum absolute values of ψ_{Ekman} across the ACC, $\Psi_{ACC} = \max_{[Y_l \le y \le L_y]} |\psi_{Ekman}|$, and across the ASF, $\Psi_{ASF} = \max_{[Y_s \le y \le Y_l]} |\psi_{Ekman}|$. These serve as a visual comparison of the compensation by ψ_{eddy} in response to changes in ψ_{mean}.

[16] Figure 3a shows that as the mid-latitude westerlies strengthen, the increased wind-driven mean overturning in the ACC is largely compensated by the eddy overturning, resulting in a relatively small increase in Ψ_{upper}. The variation of Ψ_{upper} with τ_{ACC} compares very closely with the results of *Abernathey et al.* [2011], except at τ_{ACC} = 0.1 Nm^{-2}, for which our Ψ_{upper} is around 0.15 Sv larger. A least-squares fit to the slope of Ψ_{upper} yields a sensitivity of 1.39 Sv m^2N^{-1}, which is somewhat smaller than the 2.6 Sv m^2N^{-1} calculated by *Abernathey et al.* [2011]. There is almost no discernible change in Ψ_{shelf} and Ψ_{slope}, so the deep MOC is insensitive to the strength of the mid-latitude westerlies. Similarly, Figure 3b shows that Ψ_{upper} does not vary in response to changes in τ_{ASF}, so the upper MOC is insensitive to the strength of the polar easterlies. By contrast, for easterly slope winds the variations of Ψ_{shelf} and Ψ_{slope} are comparable to that of the Ekman response Ψ_{ASF}. The least-squares slopes for Ψ_{shelf} and Ψ_{slope} in the range $\tau_{ASF} \le 0$ are 6.03 Sv m^2N^{-1} and 5.41 Sv m^2N^{-1} respectively, around four times the sensitivity of the upper MOC to the mid-latitude westerlies. This greater sensitivity is due to the suppression of baroclinic instability, the mechanism via which mesoscale eddies are generated in our model, over the continental slope [*Isachsen*, 2011]. This results in the wind-driven mean overturning ψ_{mean} dominating the MOC over the continental slope, as shown in Figure 2. The overturning on the slope is therefore strongly sensitive to changes in τ_{ASF}. Thus, because the slope connects the continental shelf and the ACC, the entire lower cell of the MOC becomes strongly sensitive τ_{ASF}. When the slope winds are westerly ($\tau_{ASF} > 0$), the eddy overturning across the slope becomes comparable in strength to the wind-driven mean overturning, so the deep MOC is relatively insensitive to wind stress changes beyond $\tau_{ASF} = 0$.

5. Discussion

[17] The deep MOC plays a crucial climatic role in ventilating the deep ocean with oxygen [*Hotinski et al.*, 2001] and storing CO_2 [*Skinner et al.*, 2010]. Changes in this circulation with climate have recently been attributed to shifting/strengthening of the mid-latitude westerlies [*Toggweiler*, 2009], which has motivated a series of modelling studies investigating the sensitivity of the MOC to westerly wind stress [*Meredith et al.*, 2011; *Abernathey et al.*, 2011]. Our results demonstrate that the deep overturning cell is much more sensitive to the polar easterlies, associated with the atmospheric polar cell, than the mid-latitude westerlies, associated with the atmospheric Ferrel cell. The sensitivity of AABW export to the polar easterlies is consistent with the idealized basin model of *Kida* [2011], in which AABW outflow is geostrophically controlled by a strait on the continental shelf.

[18] We conclude that an accurate consideration of the deep MOC in past and future climates must account for the influence of both the mid-latitude westerlies and the polar easterlies. Additional research is required to determine how this sensitivity is modified by the inclusion of realistic temperature/salinity forcing at the surface and on the shelf, and by topographic variations that may support cross-slope geostrophic currents and extract momentum from the zonal flow by form drag. Furthermore, it remains to be determined how changes in the polar easterlies and mid-latitude westerlies affect the volume and extent of the deep overturning, which ultimately determine how much CO_2 may be stored in the deep ocean.

[19] **Acknowledgments.** A.L.S.'s and A.F.T.'s research was supported by the California Institute of Technology. The simulations presented herein were conducted using the CITerra computing cluster in the Division of Geological and Planetary Sciences at the California Institute of Technology, and the authors thank the CITerra technicians for facilitating this work. The authors gratefully acknowledge the modelling efforts of the MITgcm team. The authors would like to thank Dimitris Menemenlis, Chris Wolfe, Rick Salmon and Paul Dellar for useful discussions that improved the original draft of this article. The authors would also like to thank three anonymous referees whose suggestions improved the manuscript.

[20] The Editor thanks two anonymous reviewers for assisting in the evaluation of this paper.

References

Abernathey, R., J. Marshall, and D. Ferreira (2011), The dependence of Southern Ocean meridional overturning on wind stress, *J. Phys. Oceanogr.*, *41*, 2261–2278.

Böning, C. W., A. Dispert, M. Visbeck, S. R. Rintoul, and F. U. Schwarzkopf (2008), The response of the Antarctic Circumpolar Current to recent climate change, *Nat. Geosci.*, *1*(12), 864–869.

Döös, K., and D. J. Webb (1994), The Deacon cell and the other meridional cells of the Southern Ocean, *J. Phys. Oceanogr.*, *24*, 429–429.

Ferreira, D., J. Marshall, and P. Heimbach (2005), Estimating eddy stresses by fitting dynamics to observations using a residual-mean ocean circulation model and its adjoint, *J. Phys. Oceanogr.*, *35*(10), 1891–1910.

Gordon, A. L. (2009), Bottom water formation, in *Ocean Currents*, edited by J. H. Steele, S. A. Thorpe, and K. K. Turekian, pp. 263–269, Elsevier, London.

Hofmann, M., and M. A. Morales Maqueda (2011), The response of Southern Ocean eddies to increased midlatitude westerlies: A non-eddy resolving model study, *Geophys. Res. Lett.*, *38*, L03605, doi:10.1029/2010GL045972.

Hotinski, R. M., K. L. Bice, L. R. Kump, R. G. Najjar, and M. A. Arthur (2001), Ocean stagnation and end-Permian anoxia, *Geology*, *29*(1), 7–10.

Isachsen, P. E. (2011), Baroclinic instability and eddy tracer transport across sloping bottom topography: How well does a modified Eady model do in primitive equation simulations?, *Ocean Modell.*, *39*(1), 183–199.

Jacobs, S. S. (1991), On the nature and significance of the Antarctic Slope Front, *Mar. Chem.*, *35*(1), 9–24.

Kida, S. (2011), The impact of open oceanic processes on the Antarctic Bottom Water outflows, *J. Phys. Oceanogr.*, *41*(10), 1941–1957.

Kitoh, A., S. Murakami, and H. Koide (2001), A simulation of the Last Glacial Maximum with a coupled atmosphere-ocean GCM, *Geophys. Res. Lett*, *28*(11), 2221–2224.

Kuhlbrodt, T., A. Griesel, M. Montoya, A. Levermann, M. Hofmann, and S. Rahmstorf (2007), On the driving processes of the Atlantic meridional overturning circulation, *Rev. Geophys.*, *45*, RG2001, doi:10.1029/2004RG000166.

Large, W. G., and S. G. Yeager (2009), The global climatology of an interannually varying air–sea flux data set, *Clim. Dyn.*, *33*(2), 341–364.

Large, W. G., J. C. McWilliams, and S. C. Doney (1994), Oceanic vertical mixing: A review and a model with a nonlocal boundary layer parameterization, *Rev. Geophys.*, *32*(4), 363–404.

Leith, C. E., B. Galerpin, and S. A. Orszag (1996), Large eddy simulation of complex engineering and geophysical flows, *Physica D*, *98*, 481–491.

Lumpkin, R., and K. Speer (2007), Global ocean meridional overturning, *J. Phys. Oceanogr.*, *37*(10), 2550–2562.

Lynch-Stieglitz, J., et al. (2007), Atlantic meridional overturning circulation during the Last Glacial Maximum, *Science*, *316*(5821), 66–69.

Marshall, J., and T. Radko (2003), Residual-mean solutions for the Antarctic Circumpolar Current and its associated overturning circulation, *J. Phys. Oceanogr.*, *33*(11), 2341–2354.

Marshall, J., and K. Speer (2012), Closure of the meridional overturning circulation through Southern Ocean upwelling, *Nat. Geosci.*, *5*(3), 171–180.

Marshall, J., A. Adcroft, C. Hill, L. Perelman, and C. Heisey (1997), A finite-volume, incompressible Navier Stokes model for studies of the ocean on parallel computers, *J. Geophys. Res.*, *102*, 5753–5766.

McIntosh, P. C., and T. J. McDougall (1996), Isopycnal averaging and the residual mean circulation, *J. Phys. Oceanogr.*, *26*(8), 1655–1660.

Meredith, M. P., A. C. Naveira Garabato, A. M. C. Hogg, and R. Farneti (2011), Sensitivity of the overturning circulation in the Southern Ocean to decadal changes in wind forcing, *J. Clim.*, *25*, 99–110.

Muench, R. D., and A. L. Gordon (1995), Circulation and transport of water along the western Weddell Sea margin, *J. Geophys. Res.*, *100*, 18,503–18,515.

Nowlin, Jr., W. D., and J. M. Klinck (1986), The physics of the Antarctic circumpolar current, *Rev. Geophys.*, *24*(3), 469–491.

Nurser, A. J. G., and M. M. Lee (2004), Isopycnal averaging at constant height. Part I: The formulation and a case study, *J. Phys. Oceanogr.*, *34*(12), 2721–2739.

Polvani, L. M., D. W. Waugh, G. J. P. Correa, and S. W. Son (2011), Stratospheric ozone depletion: The main driver of twentieth-century atmospheric circulation changes in the Southern Hemisphere, *J. Clim.*, *24*(3), 795–812.

Shindell, D. T., and G. A. Schmidt (2004), Southern Hemisphere climate response to ozone changes and greenhouse gas increases, *Geophys. Res. Lett.*, *31*, L18209, doi:10.1029/2004GL020724.

Skinner, L., S. Fallon, C. Waelbroeck, E. Michel, and S. Barker (2010), Ventilation of the deep Southern Ocean and deglacial CO_2 rise, *Science*, *328*(5982), 1147–1151.

Speer, K., S. R. Rintoul, and B. Sloyan (2000), The diabatic Deacon cell, *J. Phys. Oceanogr.*, *30*(12), 3212–3222.

Thompson, A. F., and K. J. Heywood (2008), Frontal structure and transport in the northwestern Weddell Sea, *Deep Sea Res., Part I*, *55*(10), 1229–1251.

Thompson, D., J. Wallace, and G. Hegerl (2000), Annular modes in the extratropical circulation. Part II: Trends, *J. Clim.*, *13*(5), 1018–1036.

Toggweiler, J. R. (2009), Shifting westerlies, *Science*, *323*(5920), 1434–1435.

Vallis, G. K. (2006), *Atmospheric and Oceanic Fluid Dynamics: Fundamentals and Large-Scale Circulation*, Cambridge Univ. Press, Cambridge, U. K.